CORA Cork Open Research Archive
Cartlann Taighde Oscailte Chorcaí

Title	Electric-field-induced interlayer hybridization and switching in bilayer PtTe2 field-effect transistors
Authors	Jamalzadeh Kheirabadi, Sharieh;Ansari, Lida;Grønbjerg Vej-Hansen, Ulrik;Hurley, Paul K.;Gity, Farzan
Publication date	2026-09-01
Original Citation	Jamalzadeh Kheirabadi, S, Ansari, L, Grønbjerg Vej-Hansen, U, Hurley, P K & Gity, F 2026, 'Electric-field-induced interlayer hybridization and switching in bilayer PtTe 2 field-effect transistors', Materials Today Electronics, vol. 17, 100229, pp. 1-9. https://doi.org/10.1016/j.mtelec.2026.100229
Type of publication	Article (peer-reviewed)
Link to publisher's version	https://www.scopus.com/pages/publications/105043358020 - 10.1016/j.mtelec.2026.100229
Rights	© 2026, authors. Published by Elsevier Ltd. This is an open access article under the CC BY license (http://creativecommons.org/licenses/by/4.0/) - https://creativecommons.org/licenses/by/4.0/
Download date	2026-11-16 11:48:57
Item downloaded from	https://hdl.handle.net/10468/19568



University College Cork, Ireland
Coláiste na hOllscoile Corcaigh

Materials Today Electronics 17 (2026) 100229

Contents lists available at ScienceDirect

Materials Today Electronics

journal homepage: www.elsevier.com/locate/mtelec

Full Length Article

Electric-field-induced interlayer hybridization and switching in bilayer $PtTe_2$ field-effect transistors

Sharieh Jamalzadeh Kheirabadi [a,*], Lida Ansari [a,*], Ulrik Grønbjerg Vej-Hansen [b], Paul K. Hurley [a,c], Farzan Gity [a]

[a] MicroNano systems, Tyndall National Institute, University College Cork, Cork, T12 R5CP, Ireland
[b] Synopsys QuantumATK, Synopsys Denmark Aps, Copenhagen, Denmark
[c] School of Chemistry, University College Cork, Cork, Ireland

ARTICLE INFO

Keywords:
Bilayer ptte2
Gate-controlled interlayer modulation
Electric field bandgap engineering
Steep subthreshold swing
Quantum transport

ABSTRACT

Two-dimensional (2D) transition metal dichalcogenides (TMDs) offer a versatile platform for band-structure engineering and nanoelectronic device design. Among them, bilayer $PtTe_2$ resides at the boundary between metallic and semiconducting behavior, providing a unique opportunity for electrically controlled phase modulation. Here, we show that a perpendicular electric field opens a bandgap in bilayer $PtTe_2$ and modulates interlayer coupling, making an expanded semiconducting configuration energetically favorable relative to the equilibrium metallic state. Density functional theory calculations combined with electric-field-dependent nudged elastic band analysis reveal that a perpendicular field of 2.5 MV/cm shifts the interlayer energy landscape and stabilizes a semiconducting configuration with a bandgap of ~0.44 eV. Non-equilibrium Green's function transport simulations reveal that this field-control interlayer modulation simultaneously induces (i) bandgap opening, (ii) modification of band-edge curvature and effective mass, (iii) enhanced electrostatic carrier depletion, and (iv) an evolution from effectively ohmic-like carrier injection in the metallic ON state to increasingly barrier-limited injection in the semiconducting OFF state. These mechanisms explain the coexistence of a relatively steep subthreshold swing and a large ON/OFF current ratio, while preserving metallic transport in the ON regime. The device remains within the thermionic regime, improving the practical steep-slope trade-off between switching efficiency and ON-state current rather than surpassing the Boltzmann limit. These findings identify field-controlled interlayer modulation in bilayer $PtTe_2$ as a promising mechanism for improving the balance between switching efficiency and ON-state conductivity in nanoscale electronic devices.

1. Introduction

Two-dimensional (2D) materials have emerged as a versatile platform for next-generation nanoelectronics, offering unprecedented opportunities for band-structure engineering and electrostatic control of carrier transport. In particular, transition metal dichalcogenides (TMDs) provide a rich spectrum of electronic phases, ranging from semiconducting to semi-metallic behavior, making them highly attractive for logic and high-performance device applications. Among various external tuning approaches, the application of a perpendicular electric field has proven especially effective for modifying electronic properties without altering material composition.

A prototypical example is bilayer graphene, where a perpendicular electric field breaks inversion symmetry and opens a bandgap by lifting the degeneracy of the π and π* bands at the Fermi level [1,2]. This field-induced symmetry breaking illustrates how electronic phases in layered materials can be reversibly controlled through electrostatic means. Similar electric-field-driven band modulation has been explored in multilayer TMD systems. While monolayer TMDs are typically intrinsic semiconductors, multilayer configurations introduce interlayer coupling as an additional tunable degree of freedom. Previous first-principles studies have shown that perpendicular electric fields can significantly alter the band structure of bilayer and few-layer TMDs with the conventional 2H crystal structure (e.g., MoS_2, $MoSe_2$, $MoTe_2$, and WS_2), where the applied field progressively reduces the intrinsic bandgap and, at sufficiently high field strengths, can drive the gap to zero, inducing semiconductor-metal transitions at critical field strengths [3,4]. These findings highlight interlayer hybridization as a powerful

* Corresponding authors.
E-mail addresses: sharieh.jamalzadeh@tyndall.ie (S. Jamalzadeh Kheirabadi), lida.ansari@tyndall.ie (L. Ansari).

https://doi.org/10.1016/j.mtelec.2026.100229
Received 1 April 2026; Received in revised form 23 June 2026; Accepted 28 June 2026
Available online 29 June 2026
2772-9494/© 2026 The Authors. Published by Elsevier Ltd. This is an open access article under the CC BY license (http://creativecommons.org/licenses/by/4.0/).

handle for electronic phase control.

Among group-10 noble TMDs, platinum ditelluride ($PtTe_2$) represents a particularly intriguing system due to its high electrical conductivity [5], environmental stability [6], and thickness-dependent electronic structure [7–9]. Unlike conventional semiconducting TMDs, $PtTe_2$ undergoes a dimensionality-driven electronic transition: while monolayer $PtTe_2$ behaves as a semiconductor, bilayer and thicker films exhibit semi-metallic characteristics [8,9]. $PtTe_2$ intrinsically adopts the 1T crystal structure [10,11], which differs fundamentally from the 2H structure typical of group-6 TMDs, giving rise to distinct interlayer hybridization and thickness-dependent electronic behavior. This intrinsic proximity to a metal-semiconductor boundary makes bilayer $PtTe_2$ an attractive candidate for electrically induced phase modulation. Importantly, the relatively weak van der Waals interaction between layers suggests that interlayer coupling may be actively tuned by an externally applied electric field, providing a potential pathway for field-controlled interlayer modulation.

Despite advances in electric-field bandgap engineering, achieving steep switching characteristics in field-effect transistors while preserving high ON-state current remains a central challenge in high-performance electronics. In many steep-slope device concepts, enhanced switching arises from transport mechanisms that inherently restrict ON-state conduction, leading to a practical trade-off between subthreshold swing and drive current. Overcoming this limitation requires a mechanism that enhances switching efficiency and improves the ON/OFF current ratio without degrading intrinsic transport properties in the ON state. Such a balance is critical for meeting the switching requirements outlined in the International Roadmap for Devices and Systems (IRDS) 2028 targets for future logic technologies [12].

Here, we demonstrate that bilayer $PtTe_2$ supports such a mechanism through gate-field-controlled modulation of interlayer coupling. By applying a perpendicular electric field, the interlayer energy landscape is modified, making an expanded semiconducting configuration energetically favorable relative to the equilibrium metallic state. This field-controlled interlayer modulation simultaneously leads to bandgap opening, modification of band-edge curvature and effective mass, and enhanced electrostatic carrier depletion. In the metallic ON state, the channel preserves high conductivity and supports effectively ohmic-like carrier injection between source, channel, and drain. As the gate field drives the system into the semiconducting regime, carrier injections become increasingly barrier-limited, further suppressing OFF-state current. The combined effect explains the coexistence of a relatively steep subthreshold swing and a large ON/OFF current ratio while preserving ON-state performance.

In this work, we employ density functional theory (DFT), nudged elastic band (NEB) calculations incorporating an external electric field, and non-equilibrium Green's function (NEGF) transport simulations to systematically investigate the structural, electronic, and transport properties of bilayer $PtTe_2$ under perpendicular electric fields. We quantify the critical electric field required to modulate the interlayer distance, analyze the resulting bandgap evolution, and evaluate device-level implications for nanoscale transistor configurations. These results identify field-controlled interlayer modulation in bilayer $PtTe_2$ as a promising route for improving the balance between ON-state conductivity and OFF-state suppression in nanoscale electronic devices.

While electric-field-induced band structure modulation has been widely explored in bilayer graphene and TMD systems, these approaches typically involve tuning the electronic structure at a fixed atomic configuration. In contrast, the present work identifies a distinct mechanism in which the applied electric field modifies the interlayer energy landscape, enabling a transition between structurally distinct configurations with different electronic phases. This field-controlled structural electronic coupling allows access to both metallic and semiconducting regimes within the same material system, providing a potential pathway to mitigate the conventional trade-off between ON-state current and switching performance in nanoscale devices.

2. Results

2.1. Quantum confinement and dimensionality-driven electronic transition in $ptte_2$

Fig. 1 presents the optimized atomic structures and orbital-resolved band structures of monolayer and bilayer $PtTe_2$. The monolayer configuration exhibits a finite bandgap of 0.87 eV, consistent with its intrinsic semiconducting nature [7,11]. The projected band structure reveals that the states near the valence- and conduction-band edges arise predominantly from hybridized Te-*p* states at the valence-band maximum (VBM) and mixed Te-*p*/Pt-*d* states at the conduction-band minimum (CBM), reflecting strong in-plane bonding interactions within the layer. The opening of the bandgap in the monolayer can be attributed to quantum confinement and the absence of interlayer hybridization, which preserves the separation between valence and conduction states. In contrast, the bilayer configuration displays a distinctly different electronic character. As shown in Fig. 1 (right panel), the bilayer band structure exhibits band overlaps, indicating semi-metallic behavior. Compared to the monolayer, additional band splitting and modified dispersion emerge due to interlayer coupling between adjacent $PtTe_2$ sheets. This interlayer hybridization alters the electronic structure and eliminates the bandgap observed in the monolayer. The corresponding orbital-resolved projected density of states (DOS) for both configurations are provided in Figure S1 in the Supporting Information (SI), where a similar orbital contribution - Te-*p* dominance at the valence-band edge and mixed Te-*p*/Pt-*d* character at the conduction-band edge - is observed for both monolayer and bilayer structures.

The transition from semiconducting monolayer to metallic bilayer $PtTe_2$ highlights a pronounced dimensionality-driven electronic transformation governed by interlayer interactions. The optimized interlayer distance in bilayer $PtTe_2$ is 3.01 Å, in good agreement with previously reported values [13], confirming the reliability of the structural optimization. At this equilibrium separation, the bilayer retains its intrinsic metallic character due to strong interlayer hybridization. For clarity in the following discussion, this equilibrium metallic configuration is denoted as $BL(d_0)$ and serves as the reference state for analyzing electric-field-induced structural and electronic evolution.

2.2. Interlayer distance and bandgap emergence in bilayer $ptte_2$

To systematically investigate the role of interlayer separation in governing the electronic properties of bilayer $PtTe_2$, we performed a controlled interlayer-distance sweep by increasing the spacing between the two layers from the equilibrium configuration $BL(d_0)$ (3.01 Å) toward expanded configurations $BL(d_{1a})$ (3.20 Å), $BL(d_{1b})$ (3.40 Å), and $BL(d_2)$ (3.64 Å), as summarized in Fig. 2. Starting from $BL(d_0)$, the bilayer retains its intrinsic metallic character ($E_g = 0$), while progressive interlayer expansion drives a clear electronic transition characterized by bandgap opening and systematic widening of the gap with separation. As shown in Fig. 2, a finite bandgap emerges at $BL(d_{1a})$ ($E_g \approx 0.17$ eV), increases at $BL(d_{1b})$ ($E_g \approx 0.33$ eV), and reaches $E_g \approx 0.44$ eV for $BL(d_2)$, establishing an interlayer-separation-driven metal-semiconductor transition in bilayer $PtTe_2$. In all band-structure insets, the energy is referenced to the Fermi level ($E_F = 0$ eV).

The accompanying band-structure insets in Fig. 2 show that the metallic band overlap at $BL(d_0)$ progressively diminishes with increasing interlayer distance, and the conduction- and valence-band edges separate to form a semiconducting gap in $BL(d_2)$. This evolution indicates that interlayer coupling is the key parameter controlling the electronic phase in bilayer $PtTe_2$, a relationship that has not previously been quantitatively correlated with controlled interlayer separation for this material. Increasing separation reduces interlayer hybridization, which suppresses band overlap near E_F and restores a semiconducting electronic structure.

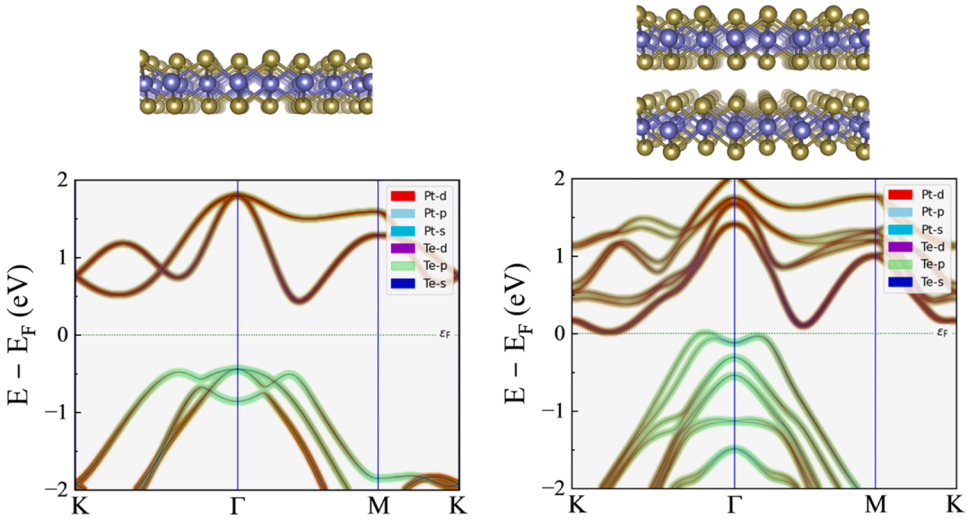


Fig. 1. Dimensionality-driven electronic transition in monolayer and bilayer $PtTe_2$. Side view and orbital-resolved band structure of (left) monolayer $PtTe_2$, exhibiting semiconducting behavior, and (right) bilayer $PtTe_2$, showing band overlap due to interlayer hybridization. The equilibrium bilayer configuration corresponds to BL(d_0). In both panels, the energy is referenced to the Fermi level (E_F = 0 eV).

To directly visualize the change in interlayer electronic interaction, Fig. 2 also presents charge density difference (CDD) maps for BL(d_0) and BL(d_2), shown as 2D distributions (isovalue = 0.05 $Å^{-3}$) together with zoomed-in views of the interlayer region. In BL(d_0), a stronger interlayer charge redistribution is observed in the region between the layers, consistent with enhanced orbital overlap and hybridization that supports metallic band overlap. In contrast, for BL(d_2) the interlayer CDD intensity is substantially reduced, indicating weakened interlayer electronic coupling at larger separation. This trend is further quantified by the line projection of the CDD extracted along a lateral direction within the interlayer mid-plane (top panel of Fig. 2), which shows a significantly larger peak amplitude for BL(d_0) compared with BL(d_2). The larger peak amplitude in BL(d_0) reflects stronger interlayer charge redistribution compared to BL(d_2). Together, the CDD analysis provides real-space microscopic evidence that the bandgap opening in Fig. 2 originates from the suppression of interlayer hybridization as the two $PtTe_2$ layers are separated.

To further elucidate the orbital origin of the emerging bandgap, we analyzed the orbital-resolved DOS for BL(d_{1a}), BL(d_{1b}), and BL(d_2), as presented in Figure S2 in the SI. For comparison, the corresponding orbital-resolved DOS of the equilibrium metallic configuration BL(d_0) is shown in Figure S1. The results indicate that the CBM is predominantly derived from mixed Te-*p*/Pt-*d* states, whereas the VBM is mainly composed of Te-*p* states across all configurations. Notably, while the dominant orbital character at the band edges remains preserved throughout the interlayer expansion, the projected DOS (PDOS) intensity near the band edges decreases and becomes less sharply defined as the interlayer distance is reduced toward BL(d_0). This reduction reflects enhanced interlayer hybridization and spectral redistribution in the closely spaced configuration, which promotes band overlap and metallic behavior. Conversely, interlayer expansion restores sharper and more pronounced band-edge features, facilitating energetic separation between valence and conduction states and enabling bandgap opening.

The persistence of orbital identity together with the modulation of DOS intensity indicates that the metal-semiconductor transition is governed primarily by changes in interlayer hybridization strength rather than by a reordering of orbital contributions at the band edges. This orbital-resolved analysis provides complementary insight beyond the CDD maps, revealing how controlled interlayer separation tunes the spectral distribution and electronic phase of bilayer $PtTe_2$. To our knowledge, such a quantitative correlation between interlayer distance, bandgap evolution, and orbital-resolved spectral redistribution has not been previously reported for bilayer $PtTe_2$.

2.3. *Electric-field-induced energetic favorability of the expanded interlayer configuration*

Having established in Fig. 2 that increasing the interlayer separation drives a metal-semiconductor transition in bilayer $PtTe_2$, we next examine how an external electric field modifies the interlayer energy landscape and the relative stability of the metallic and semiconducting configurations. To this end, nudged elastic band (NEB) calculations were performed under varying perpendicular electric field strengths to evaluate how the interlayer energy landscape evolves with applied field. Fig. 3 presents the calculated relative energy profiles as a function of interlayer separation for electric fields of 0, 1.0, 2.0, and 2.5 MV/cm.

In the absence of an external field, the equilibrium configuration BL(d_0) (3.01 Å) corresponds to the global minimum, while expansion toward BL(d_2) (3.64 Å) requires an energy increase of ~ 0.151 eV. This confirms that, under zero-field conditions, the metallic BL(d_0) configuration is energetically preferred. As a perpendicular electric field is applied, the relative energy landscape is progressively modified. With increasing field strength, the energy cost associated with interlayer expansion decreases.

At an applied field of 2.5 MV/cm (= 0.25 V/nm) [14], the relative total energy of the expanded configuration BL(d_2) drops below that of BL(d_0), indicating that the semiconducting configuration becomes thermodynamically favorable under the applied field. Importantly, this does not imply the disappearance of an activation barrier, but rather a field-induced shift in the relative total energies that alters the preferred structural state.

Physically, the perpendicular electric field introduces an electrostatic potential difference across the bilayer, effectively modifying the interlayer interaction and reducing the energetic preference for the closely spaced configuration. This electrostatic perturbation weakens interlayer hybridization, consistent with the suppression of charge redistribution and the modulation of band-edge PDOS intensity discussed in Section B. Consequently, the semiconducting configuration identified in the interlayer-distance sweep becomes energetically accessible under experimentally relevant electric field strengths. Together, Fig. 2 and Fig. 3 establish a direct quantitative link between interlayer separation, electronic phase transition, and applied electric field. The metal-semiconductor transition in bilayer $PtTe_2$ can therefore be viewed as a field-controllable energetic reconfiguration of the

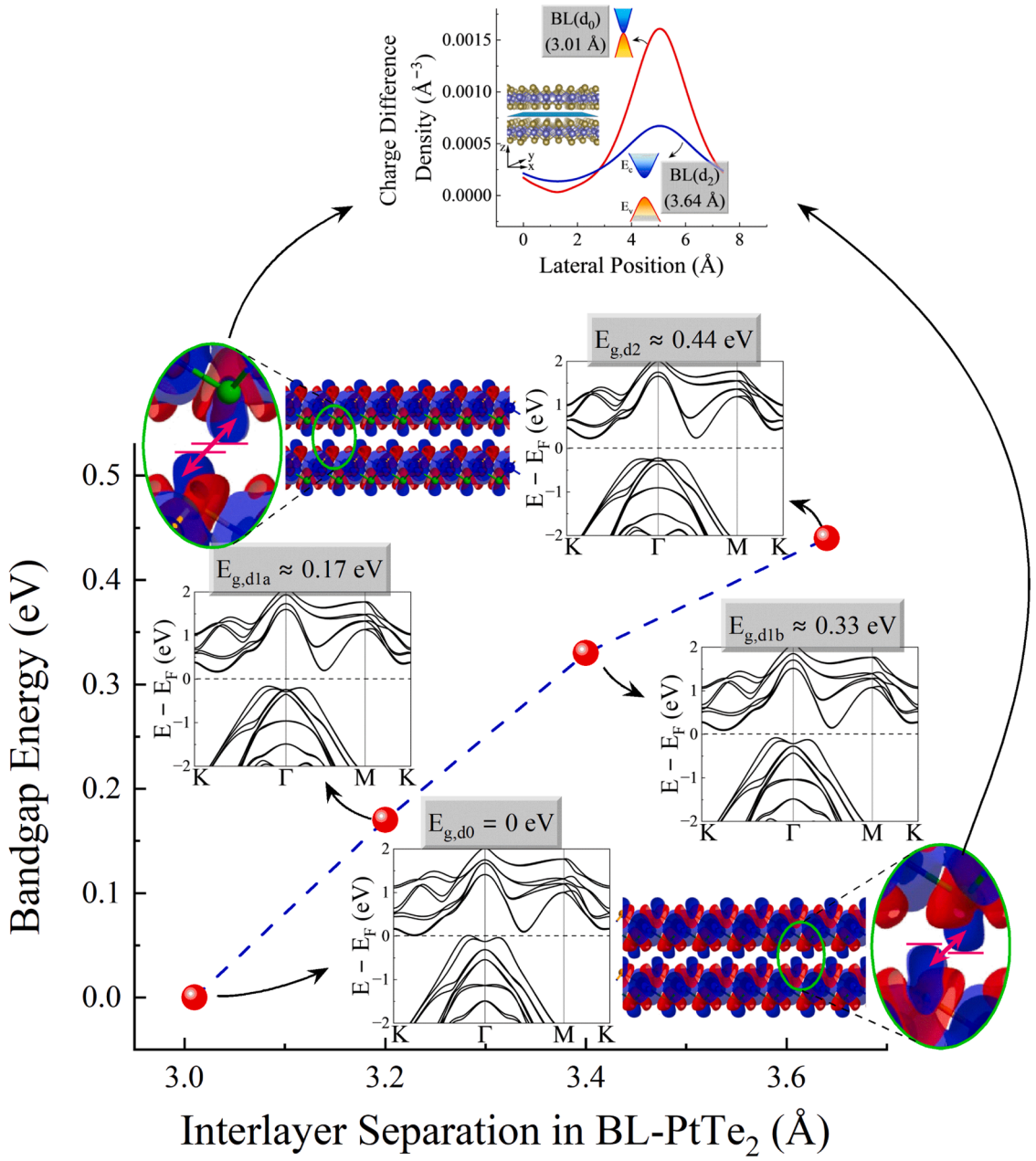


Fig. 2. Quantitative correlation between interlayer separation and bandgap opening in bilayer $PtTe_2$. Bandgap energy as a function of interlayer separation in BL-$PtTe_2$, illustrating the transition from metallic BL(d_0) to semiconducting BL(d_2). Insets show the corresponding electronic band structures for BL(d_0), BL(d_{1a}), BL(d_{1b}), and BL(d_2), demonstrating the progressive opening of the bandgap with increasing interlayer distance. In all band-structure panels, the energy is referenced to the Fermi level ($E_F = 0$ eV). Charge density difference (CDD) maps (isovalue = 0.05 Å^{-3}) for BL(d_0) and BL(d_2) visualize the change in interlayer electronic interaction. Zoomed-in views highlight the reduction of charge redistribution in the interlayer region as the separation increases. The line projection of the CDD extracted along a lateral direction within the interlayer mid-plane (top panel) quantitatively confirms the reduced interlayer charge redistribution in BL(d_2) compared with BL(d_0), providing microscopic evidence for the weakening of interlayer hybridization responsible for bandgap opening.

interlayer coupling landscape.

2.4. Gate-field-controlled metal-semiconductor transition and conceptual device operation

To evaluate the device-level implications of the electric-field-induced structural and electronic modulation described in Sections A-C, quantum transport simulations were performed using a combined DFT and NEGF framework. The simulated structure is a back-gated bilayer $PtTe_2$ field-effect transistor, shown in Fig. 4(a), consisting of bilayer $PtTe_2$ source and drain regions separated by a 13.8 nm-long channel. The channel is electrostatically controlled through a 1 nm-thick high-κ ZrO_2 gate dielectric (ε = 32). To isolate the intrinsic transport response of the channel and avoid artificial interface effects, the source and drain were modeled using uniformly doped bilayer $PtTe_2$, ensuring coherent material interfaces throughout the device.

2.4.1. Static transport characteristics of fixed interlayer configurations

Fig. 4(b) presents the calculated transfer characteristics for devices constructed using different interlayer configurations: BL(d_0), BL(d_{1a}), BL (d_{1b}), BL(d_2), along with a monolayer (ML) reference. Table 1 summarizes the corresponding electronic and transport parameters, including effective electron mass (m_e), bandgap (E_g), ON/OFF ratio, and sub-threshold swing (SS). The equilibrium metallic configuration BL(d_0),

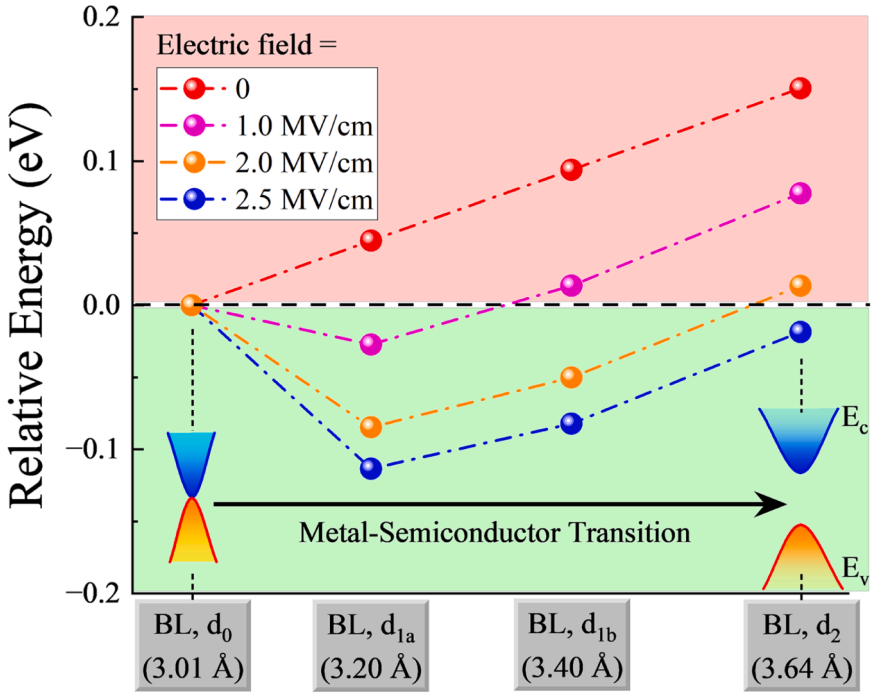


Fig. 3. Electric-field-dependent interlayer energy landscape in bilayer $PtTe_2$. NEB-calculated relative energy profiles of bilayer (BL) $PtTe_2$ as a function of interlayer separation under perpendicular electric fields of 0, 1, 2, and 2.5 MV/cm. Energy values are referenced to the equilibrium metallic configuration BL(d_0). The upper (red-shaded) region corresponds to positive relative energy with respect to BL(d_0), indicating that interlayer expansion is energetically unfavorable. The lower (green-shaded) region corresponds to negative relative energy, indicating that the expanded configuration becomes energetically favorable under the applied field. With increasing electric field strength, the relative energy of the expanded configuration decreases, and at 2.5 MV/cm (= 0.25 V/nm) BL(d_2) becomes energetically favorable relative to BL(d_0), enabling the metal-semiconductor transition identified in Fig. 2.

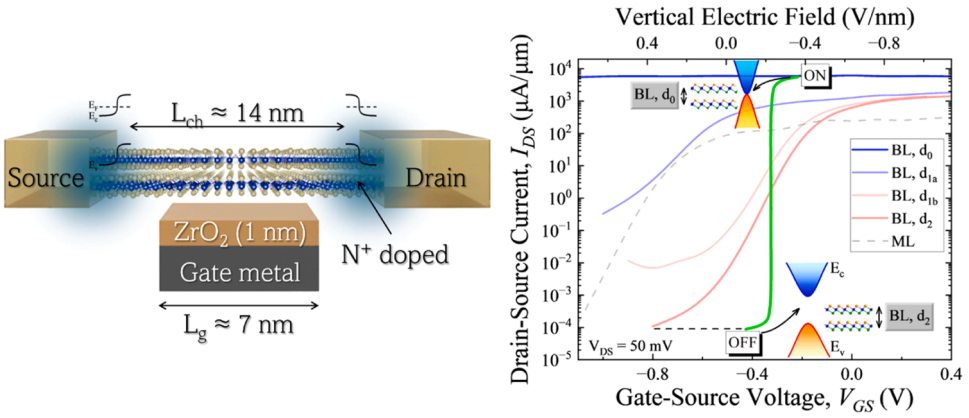


Fig. 4. Gate-controlled transport characteristics and field-controlled metal-semiconductor transition in bilayer $PtTe_2$ field-effect transistors (FETs). (a) Schematic of the simulated back-gated bilayer $PtTe_2$ FET, consisting of bilayer $PtTe_2$ source and drain regions separated by a ~14 nm-long channel and electrostatically controlled througha gate oxide represented by a 1 nm-thick high-κ ZrO_2 layer (ε = 32). (b) Calculated transfer characteristics (I_{DS}–V_{GS}) for devices constructed from fixed interlayer configurations BL(d_0), BL(d_{1a}), BL(d_{1b}), BL(d_2), and a monolayer (ML) reference. Progressive interlayer expansion leads to systematic bandgap opening and improved switching behavior. The green curve illustrates the conceptual field-controlled transition between the metallic BL(d_0) and semiconducting BL(d_2) configurations, inferred from the field-dependent energy landscape and the transport characteristics calculated for fixed interlayer separations. The bottom horizontal axis represents the applied gate bias (V_{GS}), while the top horizontal axis denotes the corresponding perpendicular electric field in the channel (V/nm), obtained through electrostatic conversion and directly related to the interlayer energetic modulation shown in Fig. 3.

characterized by zero bandgap, exhibits negligible current modulation (ON/OFF ≈ 1), confirming that the metallic channel cannot support conventional switching. As the interlayer separation increases to BL(d_{1a}) (E_g ≈ 0.17 eV), partial current suppression emerges, yielding an ON/OFF ratio of ~5.5×10^3 and SS ≈ 148 mV/dec. Further expansion to BL (d_{1b}) (E_g ≈ 0.33 eV) significantly enhances switching behaviour, with ON/OFF ≈ 2.5×10^5 and SS ≈ 93 mV/dec. In the semiconducting BL(d_2) configuration (E_g ≈ 0.44 eV), a pronounced OFF-state is obtained, resulting in ON/OFF ≈ 1.3×10^7 and SS ≈ 75 mV/dec. For comparison, the monolayer device (E_g ≈ 0.9 eV) exhibits ON/OFF ≈ 2.2×10^6 with SS ≈ 72 mV/dec.

Notably, the effective electron mass increases gradually from 0.748 m_0 in BL(d_0) to 0.767 m_0 in BL(d_2), reflecting progressive flattening of the band-edge curvature as interlayer separation increases. Since carrier

Table 1
Summary of electronic and transport parameters, including effective electron mass (m_e), bandgap (E_g), ON/OFF current ratio, and subthreshold swing (SS). The evolution from BL(d_0) to BL(d_2) shows that interlayer modulation is associated with improved switching performance while preserving high ON-state conductivity in the metallic regime.

Channel Parameter	BL (d_0)	BL (d_{1a})	BL (d_{1b})	BL (d_2)	ML
m_e	0.748	0.753	0.762	0.767	-
E_g (eV)	0	0.17	0.33	0.44	0.9
ON/OFF	~1	5.5×10^3	2.5×10^5	1.3×10^7	2.2×10^6
SS (mV/dec)	NA	148	93	75	72

mobility is inversely proportional to effective mass under comparable scattering conditions, the smaller effective mass in BL(d_0) supports higher carrier mobility and therefore higher ON-state current. Conversely, the larger effective mass in BL(d_2) contributes to reduced carrier mobility, further assisting OFF-state current suppression. These results demonstrate a systematic improvement in switching characteristics with increasing interlayer separation and bandgap opening.

Importantly, while larger bandgaps improve OFF-state suppression and SS, they typically reduce ON-state conductivity. In contrast, the bilayer $PtTe_2$ system uniquely allows access to both metallic and semiconducting regimes within the same material platform.

2.4.2. Field-controlled metal–semiconductor transition and conceptual device operation

The electronic and transport results collectively support an inferred gate-field-controlled transition between metallic and semiconducting configurations in bilayer $PtTe_2$. The green curve in Fig. 4(b) conceptually illustrates the expected device response associated with the inferred gate-induced transition between interlayer configurations. It is constructed from the field-dependent energetic preference of the bilayer configurations and the transport characteristics calculated for fixed interlayer separations. The bottom horizontal axis represents the applied gate bias (V_{GS}), while the top horizontal axis denotes the corresponding perpendicular electric field strength in the channel region (expressed in V/nm), obtained through electrostatic conversion across the gate dielectric. This electric field directly governs the interlayer expansion quantified in Fig. 3. At positive gate bias (corresponding to negative electric field values), the channel remains in the equilibrium metallic configuration BL(d_0). In this ON state, the absence of a bandgap ensures high carrier density and strong band dispersion near the Fermi level, resulting in high current conduction. As the gate voltage is swept toward negative bias, the increasing perpendicular electric field modifies the interlayer energetic preference (Section C), progressively driving the system toward expanded configurations BL(d_1) and ultimately into the semiconducting BL(d_2) regime. This structural evolution is consistent with the bandgap evolution shown in Fig. 2. The emergence of a finite bandgap, together with the modification of band-edge curvature, leads to rapid current suppression and enables a steep subthreshold transition. To relate the required perpendicular electric field to realistic device operation, we estimate the corresponding gate voltage based on the assumed dielectric thickness. For the critical field of ~2.5 MV/cm (≈ 0.25 V/nm) and a dielectric thickness of 1 nm (ZrO_2, $\varepsilon \approx 32$), the equivalent gate voltage is approximately 0.25 V using the relation $V = E \bullet t_{ox}$. This voltage is within the range considered for aggressively scaled nanoscale devices employing high-κ dielectrics. Nevertheless, practical realization will depend on dielectric breakdown strength, leakage current, interface quality, and the detailed device architecture, and further optimization may be required to reduce the operating voltage [15]. Therefore, the present estimate should be regarded as an electrostatic feasibility estimate rather than a complete gate-stack reliability assessment.

2.4.3. Physical origin of enhanced switching

The following analysis combines static electronic structure calculations, field-dependent energetic considerations, and transport simulations of fixed configurations to infer the behavior of a gate-controlled transition, rather than explicitly modeling time-dependent switching dynamics. During this gate-induced metal-semiconductor transition, current modulation arises from four concurrent mechanisms: (i) bandgap opening, which reduces intrinsic carrier concentration, (ii) modification of band-edge curvature, increasing effective mass and reducing carrier mobility, (iii) enhanced electrostatic carrier depletion under gate bias, and (iv) evolution of carrier injection characteristics. In the metallic BL(d_0) configuration, carrier injection between source, channel, and drain is effectively ohmic-like, minimizing injection resistance and preserving high ON-state conductivity. As the channel transitions toward the semiconducting BL(d_2) configuration, carrier injection becomes increasingly barrier-limited, further suppressing OFF-state current. The combined action of these mechanisms explains the coexistence of a relatively steep subthreshold swing and a large ON/OFF current ratio in the idealized transport simulations, while preserving metallic transport in the ON state. Unlike many conventional steep-slope device concepts, where enhanced switching can compromise ON-state current, the proposed gate-controlled interlayer modulation offers a potential route to improve current suppression while retaining favourable ON-state conductivity. These results should be interpreted as an intrinsic performance estimate within the coherent-transport limit.

3. Discussion

The bilayer $PtTe_2$ system offers a distinct advantage over the monolayer case by enabling access to both metallic and semiconducting regimes within the same material platform. In the equilibrium BL(d_0) configuration, the channel is metallic, providing strong electronic coupling between source, channel, and drain and thereby facilitating efficient carrier injection with minimal contact resistance. This metallic state effectively serves as a conductive anchor that preserves high ON-state current. In contrast, the monolayer is intrinsically semiconducting and therefore subject to carrier injection limitations. Upon application of a perpendicular electric field, the bilayer transitions to the semiconducting BL(d_2) configuration, which supports strong current suppression while maintaining a relatively high density of states near the band edges compared to the monolayer. This combination of a metallic ON state and a semiconducting OFF state allows the bilayer system to mitigate the conventional trade-off between ON-state current and switching sharpness, providing a more favorable balance than fixed-bandgap monolayer devices.

The device behavior discussed in this work is inferred from a combination of static electronic-structure calculations, electric-field-dependent NEB analysis of the interlayer energy landscape, and transport simulations performed for fixed structural configurations. Accordingly, the present results support the possibility of a field-controlled transition between distinct structural and electronic states, rather than providing a fully dynamic simulation of the coupled electrostatic and structural evolution. A quantitative description of the real-time switching dynamics would require more advanced time-dependent simulations, which are beyond the scope of the present study.

In bilayer $PtTe_2$, the interlayer modulation involves atomic-scale displacements (~0.6 Å) driven by the applied electric field, which modifies the interlayer energy landscape as confirmed by NEB calculations. Thus, the process should be viewed not as macroscopic mechanical motion, but as a field-induced transition between two nearby energy minima, similar to atomic-scale lattice relaxation or polarization switching in low-dimensional materials. The switching timescale would be governed by the energy barrier and phonon-limited lattice dynamics and is therefore expected to be much faster than macroscopic mechanical actuation, although it is not explicitly calculated in the present work. While potentially slower than purely electronic switching in

CMOS devices, this mechanism may be more relevant for beyond-CMOS applications, where energy efficiency and ON/OFF performance are prioritized over ultimate switching speed.

The transport simulations presented here are performed within a coherent NEGF framework and therefore represent intrinsic upper-bound estimates of the proposed device. Effects such as electron–phonon scattering, impurity scattering, defects, and finite-temperature fluctuations are not explicitly included. In realistic devices, scattering processes may reduce carrier mobility and lower the ON-state current, while scattering-induced energy broadening may degrade the subthreshold swing relative to the ideal coherent limit. Structural defects and impurities could further introduce localized states that increase OFF-state leakage and locally perturb the interlayer coupling [16–18]. In addition, finite-temperature effects may influence both carrier transport and the stability of the competing interlayer configurations. Although these effects are expected to quantitatively modify the device characteristics, the underlying mechanism of electric-field-controlled interlayer hybridization and the associated metal–semiconductor transition should remain qualitatively robust. A more comprehensive treatment including scattering, disorder, and temperature-dependent dynamics would require advanced approaches such as electron-phonon coupling calculations and molecular dynamics simulations. Therefore, the present work should be regarded as a proof-of-concept study that establishes a basis for future device optimization and experimental investigations.

It should be noted that the electric-field-induced transition between BL(d_0) and BL(d_2) occurs in the presence of a finite activation barrier, as indicated by the NEB analysis. The presence of an energy barrier between the competing interlayer configurations may lead to hysteretic behavior during forward and reverse gate sweeps, as further supported by the reverse NEB energy profile shown in Figure S3 of the SI. Such hysteresis could influence threshold-voltage reproducibility during cyclic operation. However, unlike conventional charge-trapping-induced hysteresis, the present effect originates from the field-dependent interlayer energy landscape and the coexistence of competing interlayer configurations separated by an energy barrier. Therefore, its physical origin differs from charge trapping at defects or dielectric/interface states. The magnitude of the hysteresis window, its reproducibility, and its impact on logic operation are not quantified in the present work and require future dynamic simulations or experimental gate-sweep measurements.

It is important to consider the mechanical stability of the proposed interlayer modulation under repeated operation. The field-induced transition involves variation of the interlayer distance governed by van der Waals interactions and does not require bond breaking, suggesting that the process may be mechanically accessible in principle. However, under prolonged electric-field cycling, effects such as interlayer sliding, structural fatigue, defect generation, local deformation, or gradual degradation may arise and influence device reliability. A detailed assessment of long-term stability would require further investigation, for example through molecular dynamics simulations under cyclic electric fields or experimental gate-cycling measurements, and is left for future work.

Moreover, we note that the device operation considered in this work is governed by thermionic transport and therefore does not exhibit subthreshold swing values below the Boltzmann limit of ~60 mV/dec at room temperature. In this context, the proposed mechanism addresses the practical trade-off commonly observed in transistor design, where improvements in switching behavior or OFF-state suppression are often accompanied by a reduction in ON-state current. Here, the electric-field-induced modulation of interlayer hybridization provides access to a metallic ON-state with efficient carrier injection and a semiconducting OFF-state with strong current suppression, thereby allowing relatively sharp switching behavior within the thermionic regime while preserving high ON-state conductivity. This mechanism therefore provides a pathway to mitigate the ON-current versus switching-efficiency trade-off, rather than a route to overcome the intrinsic Boltzmann limit.

4. Conclusion

In summary, we have shown that a perpendicular electric field can modify the interlayer energy landscape in bilayer $PtTe_2$, making an expanded semiconducting configuration energetically favorable relative to the equilibrium metallic state. Through systematic interlayer-separation analysis, we established that bandgap opening in bilayer $PtTe_2$ is directly governed by interlayer hybridization, a relationship that has not previously been quantitatively correlated with controlled interlayer spacing for this material. Orbital-resolved analysis further reveals that the dominant band-edge character remains Te-*p* at the valence-band maximum and mixed Te-*p*/Pt-*d* at the conduction-band minimum across all configurations, indicating that the transition is governed by modulation of hybridization strength rather than a reordering of orbital contributions. By applying an external electric field, the interlayer energy landscape is modified such that the expanded configuration becomes energetically favorable, rendering the semiconducting phase accessible under experimentally relevant field strengths (2.5 MV/cm). This gate-field-driven structural reconfiguration simultaneously induces bandgap opening, modification of band-edge curvature and effective mass, and enhanced electrostatic carrier depletion. In addition, carrier injection evolves from effectively ohmic-like transport in the metallic ON state to increasingly barrier-limited injection in the semiconducting OFF state. The combined action of these mechanisms explains the coexistence of a relatively steep subthreshold swing and a large ON/OFF current ratio, while preserving high intrinsic conductivity in the ON regime. Unlike many conventional steep-slope device concepts, where enhanced switching often comes at the expense of drive current, the proposed gate-controlled interlayer modulation leverages an intrinsic structural degree of freedom within the same material platform. These findings identify field-controlled interlayer modulation in bilayer $PtTe_2$ as a promising proof-of-concept mechanism for improving the balance between ON-state conductivity and OFF-state suppression in two-dimensional electronic devices.

5. Method

The geometry optimization and electronic structure calculations were carried out using DFT as implemented in the Synopsys QuantumATK simulation package [19]. To accurately describe the interaction between electrons and atomic cores, norm-conserving pseudopotentials obtained from the PseudoDojo library were employed along with a pseudo-atomic localized basis set (Medium) [20]. The exchange–correlation energy was described using the Perdew–Burke–Ernzerhof (PBE) functional within the generalized gradient approximation (GGA) framework [21]. During the optimization of the unit cell, the Bravais lattice type was held fixed to preserve the crystal symmetry. Structural optimization was considered converged when the maximum force was reduced below 0.02 eV/Å. A density mesh cutoff of 105 Hartree was adopted, and the self-consistent field (SCF) iterations were considered converged when the energy difference between successive steps fell below 10^{-7} Hartree.

The electronic-structure calculations were performed at the PBE level. Since PBE is known to underestimate absolute bandgap values, the calculated gaps should be interpreted quantitatively within this level of theory. The main focus of the present work is the trend in bandgap evolution with interlayer separation and applied electric field. Hybrid-functional or many-body approaches may modify the absolute bandgap values, but the qualitative interlayer-separation-driven transition from metallic to semiconducting behavior is expected to remain robust.

For bilayer $PtTe_2$ systems, van der Waals (vdW) interactions were incorporated using Grimme's DFT-D3 dispersion correction to properly account for noncovalent long-range interlayer interactions [22]. To

evaluate the energetic evolution of interlayer expansion under applied electric fields, the nudged elastic band (NEB) method [23,24] was employed. A series of intermediate images along the interlayer separation pathway were generated and iteratively optimized until the maximum force on each image was reduced below 0.02 eV/Å. The resulting relative energy profiles were referenced to the equilibrium configuration BL(d_0).

In this approach, we include the influence of the electric field following the methodology of Fu and Bellaiche [25], where the field-induced force is calculated from the Born effective charge (BEC) [26] and combined with the Hellmann–Feynman force to obtain the total force on each ion. To account for the dependence of the electrostatic response on structural configuration, the BEC is evaluated for configurations corresponding to different interlayer separations along the transition pathway. This allows the field-induced forces to reflect the evolution of the interlayer electronic environment during the structural transition. Quantum transport simulations were performed using a DFT-based non-equilibrium Green's function (NEGF) formalism as implemented in the Synopsys QuantumATK simulation package. The device structure consisted of semi-infinite bilayer $PtTe_2$ source and drain electrodes connected to a finite channel region, with electrostatic gating incorporated through a dielectric layer. The transport properties were computed self-consistently by solving the coupled Poisson and Schrödinger equations under open boundary conditions.

The drain current was calculated within the Landauer-Büttiker formalism under coherent transport conditions. In this framework, the current through the device is expressed as [27]:

$$I_D = 2e/h \int T(E,\ V_{GS}, V_{DS})\left[f_S(E) - f_D(E)\right] dE \quad (1)$$

where $T(E, V_{GS}, V_{DS})$ is the energy-dependent transmission coefficient, and $f_S(E)$ and $f_D(E)$ are the Fermi-Dirac distribution functions of the source and drain electrodes, respectively. Here, e is the elementary charge and h is Planck's constant. The transmission function was obtained from the Green's function of the device region coupled to semi-infinite electrodes through appropriate self-energies, and the coupled Poisson and Schrödinger equations were solved self-consistently to account for electrostatic gating effects.

The effective electron mass values were extracted from parabolic fitting of the conduction band minimum between the Γ and M points.

Funding

This research is supported by the Marie Skłodowska-Curie Actions (MSCA), grant agreement number 101109772. This work is also supported by Research Ireland (formerly Science Foundation Ireland) through the Frontiers for the Future PI Award (24/FFP-A/13329) and the AMBER Research Centre (SFI-12/RC/2278_P2).

CRediT authorship contribution statement

Sharieh Jamalzadeh Kheirabadi: Writing – review & editing, Writing – original draft, Visualization, Validation, Software, Project administration, Methodology, Investigation, Funding acquisition, Formal analysis, Data curation, Conceptualization. **Lida Ansari:** Writing – review & editing, Validation, Supervision, Software, Project administration, Methodology, Investigation, Funding acquisition, Formal analysis, Data curation, Conceptualization. **Ulrik Grønbjerg Vej-Hansen:** Writing – review & editing, Validation, Software, Methodology, Investigation. **Paul K. Hurley:** Validation, Investigation. **Farzan Gity:** Writing – review & editing, Visualization, Validation, Supervision, Project administration, Investigation, Funding acquisition, Formal analysis, Data curation, Conceptualization.

Declaration of competing interest

The authors declare that they have no known competing financial interests or personal relationships that could have appeared to influence the work reported in this paper.

Acknowledgement

SFI/HEA Irish Centre for High-End Computing (ICHEC) is acknowledged for the provision of computational facilities and support.

Supplementary materials

Supplementary material associated with this article can be found, in the online version, at doi:10.1016/j.mtelec.2026.100229.

Data availability

No data was used for the research described in the article.

References

[1] Q. Liu, L. Li, Y. Li, Z. Gao, Z. Chen, J. Lu, Tuning electronic structure of bilayer MoS_2 by vertical electric field: a first-principles investigation, J. Phys. Chem. C 116 (40) (2012) 21556–21562, https://doi.org/10.1021/jp307124d.
[2] E.V. Castro, et al., Electronic properties of a biased graphene bilayer, J. Phys.: Condens. Matter 22 (2010) 175503, https://doi.org/10.1088/0953-8984/22/17/175503.
[3] Q. Yue, S. Chang, J. Kang, X. Zhang, Z. Shao, S. Qin, J.J. Li, Bandgap tuning in armchair MoS2 nanoribbon, J. Phys.: Condens. Matter 24 (2012) 335501, https://doi.org/10.1088/0953-8984/24/33/335501.
[4] A. Ramasubramaniam, D. Naveh, E. Towe, Tunable band gaps in bilayer transition-metal dichalcogenides, Phys. Rev. B 84 (2011) 205325, https://doi.org/10.1103/PhysRevB.84.205325.
[5] M. Wang, et al., Wafer-scale growth of 2D $PtTe_2$ with layer orientation tunable high electrical conductivity and superior hydrophobicity, ACS. Appl. Mater. Interfaces. 12 (2020) 10839–10851, https://doi.org/10.1021/acsami.9b21838.
[6] T. Wei, et al., Mid-infrared photodetection of type-II dirac semimetal 1T-$PtTe_2$ grown by molecular beam epitaxy, ACS. Appl. Mater. Interfaces. 13 (2021) 22757–22764, https://doi.org/10.1021/acsami.1c04598.
[7] K. Zhussupbekov, L. Ansari, J.B. McManus, et al., Imaging and identification of point defects in PtTe2, npj 2D mater Appl 5 (2021) 14, https://doi.org/10.1038/s41699-020-00196-8.
[8] M.K. Lin, et al., Dimensionality-mediated semimetal-semiconductor transition in ultrathin PtTe2 films, Phys. Rev. Lett. 124 (2020) 036402, https://doi.org/10.1103/PhysRevLett.124.036402.
[9] J. Li, S. Kolekar, M. Ghorbani-Asl, T. Lehnert, J. Biskupek, U. Kaiser, A. V. Krasheninnikov, M. Batzill, Layer-dependent band gaps of platinum dichalcogenides, ACS. Nano 15 (2021) 13249–13259, https://doi.org/10.1021/acsnano.1c02971.
[10] R.A.B. Villaos, C.P. Crisostomo, Z.Q. Huang, et al., Thickness dependent electronic properties of Pt dichalcogenides, NPJ. 2D. Mater. Appl. 3 (2019) 2, https://doi.org/10.1038/s41699-018-0085-z.
[11] L. Zhang, et al., MBE-grown ultrathin $PtTe_2$ films and their layer-dependent electronic structures, Nanoscale 14 (2022) 7650–7658, https://doi.org/10.1039/D2NR00944G.
[12] L. Ansari, et al., Correlation of TMD Defects with Device Performance in Ultra-Scaled Channels: Theoretical Insights and Experimental Observations, 2024 IEEE International Electron Devices Meeting (IEDM), San Francisco, CA, USA, 2024, pp. 1–4, https://doi.org/10.1109/IEDM50854.2024.10873322.
[13] L. Han, et al., Strong interlayer interaction in two-dimensional layered $PtTe_2$, J. Solid. State Chem. 305 (2022) 122657, https://doi.org/10.1016/j.jssc.2021.122657. ISSN 0022-4596.
[14] B.I. Weintrub, Y.L. Hsieh, S. Kovalchuk, et al., Generating intense electric fields in 2D materials by dual ionic gating, Nat. Commun. 13 (2022) 6601, https://doi.org/10.1038/s41467-022-34158-z.
[15] B. Wang, W. Huang, L. Chi, M. Al-Hashimi, T.J. Marks, A. Facchetti, High-k gate dielectrics for emerging flexible and stretchable electronics, Chem. Rev. 118 (11) (2018) 5690–5754, https://doi.org/10.1021/acs.chemrev.8b00045.
[16] A. Martinez, A. Price, R. Valin, et al., Impact of phonon scattering in Si/GaAs/InGaAs nanowires and FinFets: a NEGF perspective, J. Comput. Electron. 15 (2016) 1130–1147, https://doi.org/10.1007/s10825-016-0851-0.
[17] M.S. Lundstrom, J. Guo, Nanoscale transistors: device physics, modeling and simulation VII 217, Sprinber, Berlin, 2006, https://doi.org/10.1007/0-387-28003-0 p. p. 0-387-28002-2.
[18] P. Long, J.Z. Huang, Z. Jiang, G. Klimeck, M.J.W. Rodwell, M. Povolotskyi, Performance degradation of superlattice MOSFETs due to scattering in the contacts, J. Appl. Phys. 120 (22) (2016) 224501, https://doi.org/10.1063/1.4971341.

[19] S. Smidstrup, et al., QuantumATK: an integrated platform of electronic and atomic-scale modelling tools, J. Phys. Condes. Matter 32 (2020) 015901, https://doi.org/10.1088/1361-648X/ab4007.
[20] M.J. van Setten, M. Giantomassi, E. Bousquet, M.J. Verstraete, D.R. Hamann, X. Gonze, G.-M. Rignanese, The PseudoDojo: training and grading a 85 element optimized norm-conserving pseudopotential table, Comput. Phys. Commun. 226 (2018) 39–54, https://doi.org/10.1016/j.cpc.2018.01.012. ISSN 0010-4655.
[21] J.P. Perdew, K. Burke, M. Ernzerhof, Generalized gradient approximation made simple, Phys. Rev. Lett. 77 (1996) 3865–3868, https://doi.org/10.1103/PhysRevLett.77.3865.
[22] S. Grimme, J. Antony, S. Ehrlich, H. Krieg, A consistent and accurate ab initio parametrization of density functional dispersion correction (DFT-D) for the 94 elements H-Pu, J. Chem. Phys. 132 (15) (2010) 154104, https://doi.org/10.1063/1.3382344.
[23] H. Jónsson, G. Mills, K.W. Jacobsen, Nudged elastic band method for finding minimum energy paths of transitions, World Scientific, Singapore (1998) 385–404, https://doi.org/10.1142/9789812839664_0016.
[24] G. Henkelman, B.P. Uberuaga, H. Jónsson, A climbing image nudged elastic band method for finding saddle points and minimum energy paths, J. Chem. Phys. 113 (2000) 9901–9904, https://doi.org/10.1063/1.1329672.
[25] H. Fu, L. Bellaiche, First-principles determination of electromechanical responses of solids under finite electric fields, Phys. Rev. Lett. 91 (5) (2003) 057601, https://doi.org/10.1103/PhysRevLett.91.057601.
[26] R.D. King-Smith, &.D. Vanderbilt, Theory of polarization of crystalline solids, Phys. Rev. B 47 (3) (1993) 1651–1654, https://doi.org/10.1103/PhysRevB.47.1651.
[27] R. Landauer, Spatial variation of currents and fields due to localized scatterers in metallic conduction, IBM. J. Res. Dev. 1 (1957) 223–231, https://doi.org/10.1147/rd.13.0223.